JACS
JOURNAL OF THE AMERICAN CHEMICAL SOCIETY
Cite This: J. Am. Chem. Soc. 2019, 141, 19964−19968
Communication
pubs.acs.org/JACS

Engineering the Electronic Structure of Submonolayer Pt on Intermetallic Pd_3Pb via Charge Transfer Boosts the Hydrogen Evolution Reaction

Yancai Yao,[†,○] Xiang-Kui Gu,[§,○] Dongsheng He,[∥,○] Zhijun Li,[⊥] Wei Liu,[#] Qian Xu,[#] Tao Yao,[#] Yue Lin,[†] Hui-Juan Wang,[†] Changming Zhao,[†] Xiaoqian Wang,[†] Peiqun Yin,[†] Hai Li,[▽] Xun Hong,[†] Shiqiang Wei,[#] Wei-Xue Li,[†] Yadong Li,[†,‡] and Yuen Wu*[,†]

[†]Department of Chemistry, Hefei National Laboratory for Physical Sciences at the Microscale, iChEM (Collaborative Innovation Center of Chemistry for Energy Materials), University of Science and Technology of China, Hefei 230026, China

[‡]Department of Chemistry and Collaborative Innovation Center for Nanomaterial Science and Engineering, Tsinghua University, Beijing 100084, China

[§]School of Power and Mechanical Engineering, Wuhan University, Wuhan 430072, China

[∥]Materials Characterization and Preparation Center (MCPC), Southern University of Science and Technology (SUSTech), Shenzhen 518055, China

[⊥]Provincial Key Laboratory of Oil & Gas Chemical Technology, College of Chemistry and Chemical Engineering, Northeast Petroleum University, Daqing 163318, China

[#]National Synchrotron Radiation Laboratory, University of Science and Technology of China, Hefei 230026, China

[▽]Key Laboratory of Flexible Electronics (KLOFE) and Institute of Advanced Materials (IAM), Jiangsu National Synergetic Innovation Center for Advanced Materials (SICAM), Nanjing Technology University, Nanjing, Jiangsu 211816, China

Supporting Information

ABSTRACT: The efficient electrochemical hydrogen evolution reaction (HER) plays a key role in accelerating sustainable H_2 production from water electrolysis, but its large-scale applications are hindered by the high cost of the state-of-the-art Pt catalyst. In this work, submonolayer Pt was controllably deposited on an intermetallic Pd_3Pb nanoplate (AL-Pt/Pd_3Pb). The atomic efficiency and electronic structure of the active surface Pt layer were largely optimized, greatly enhancing the acidic HER. AL-Pt/Pd_3Pb exhibits an outstanding HER activity with an overpotential of only 13.8 mV at 10 mA/cm^2 and a high mass activity of 7834 A/g_{Pd+Pt} at −0.05 V, both largely surpassing those of commercial Pt/C (30 mV, 1486 A/g_{Pt}). In addition, AL-Pt/Pd_3Pb shows excellent stability and robustness. Theoretical calculations show that the improved activity is mainly derived from the charge transfer from Pd_3Pb to Pt, resulting in a strong electrostatic interaction that can stabilize the transition state and lower the barrier.

Hydrogen as a clean energy carrier in fuel cells is industrially produced from carbon feedstocks via various processes,[1−4] which are environmentally unfriendly because of the release of CO_2. The electrochemical hydrogen evolution reaction (HER) in water electrolysis is an alternative way to produce H_2.[5−7] The HER involving the reduction of H^+ and desorption of H_2 plays a key role in the water splitting process.[8−10] The design of highly active and stable electrocatalysts is a prerequisite for the HER process. Currently, this process is still largely limited to the use of precious metals such as Pt, especially for industrial requirements.[11,12] This largely increases the cost of electrolyzers and prevents their large-scale applications.

Numerous efforts to lower the cost of these metals via tuning the compositions and morphologies by increasing their atomic efficiency and intrinsic activity have been reported.[13−16] Since the surface atoms always play a dominant role in the catalytic process, deposition of a precious metal monolayer or submonolayer on a nonprecious substrate is an ideal strategy to extremely enhance the mass activity.[17,18] However, it is worth noting that stability problems of catalyst would apparently emerge when the as-grown layer is reduced to the atomic scale.[19,20] To solve this problem, choosing a chemically stable substrate that can resist acid etching and finding an effective surface engineering tool to greatly enhance the interaction between substrate and as-grown atomic overlayer are crucial to the catalyst design.[21,22]

In this work, an intermetallic Pd_3Pb nanoplate was selected as the substrate because of its excellent chemical resistance to acidic corrosion, which results from its stable and strictly ordered atomic arrangement.[23,24] First, the Pd_3Pb nanoplates were successfully prepared, and the X-ray diffraction (XRD) pattern (Figure S1) indicated that the intermetallic phase was obtained. Low-magnification high-angle annular dark-field scanning transmission electron microscopy (HAADF-STEM) (Figures 1A) and TEM (Figure S2) images showed that the Pd_3Pb nanoplates presented a square morphology enclosed by

Received: September 9, 2019
Published: December 5, 2019

DOI: 10.1021/jacs.9b09391
J. Am. Chem. Soc. 2019, 141, 19964−19968

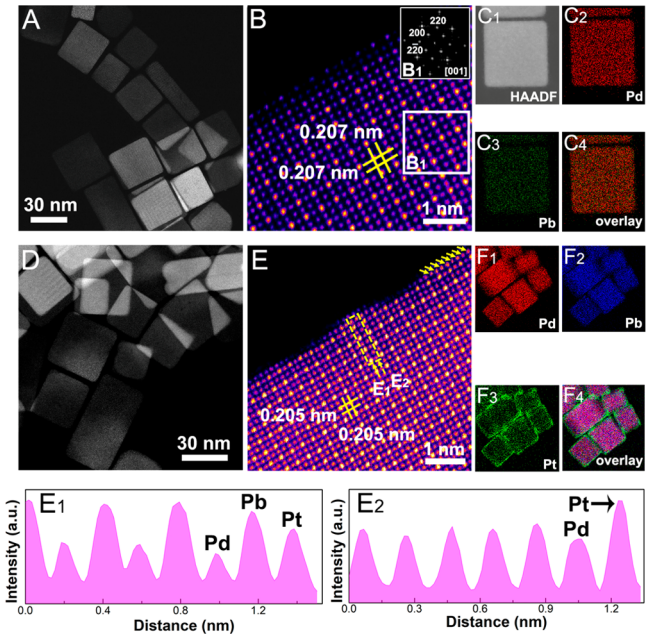

Figure 1. (A) HAADF-STEM image, (B) atomic-resolution HAADF-STEM image and FFT pattern, and (C) EDS mapping of Pd_3Pb. (D) HAADF-STEM and (E) atomic-resolution HAADF-STEM images of AL-Pt/Pd_3Pb. (E_1, E_2) Line intensity profiles taken along the yellow dashed arrow direction in (E). (F) EDS mapping of AL-Pt/Pd_3Pb.

{100} facets, which was further confirmed by the electron diffraction pattern (Figure S3) and fast Fourier transform (FFT) pattern (Figure 1B_1). According to the atomic force microscopy (AFM) image (Figure S4), the thickness of the Pd_3Pb nanoplates was estimated to be 7 nm and the height to width ratio was about 0.17. The atomic resolution HAADF-STEM image (Figure 1B) shows a characteristic lattice spacing of 0.207 nm, which was assigned to the {200} facets of Pd_3Pb. EDS mapping (Figure 1C) revealed that Pd and Pb were distributed uniformly, further demonstrating the intermetallic structure.

Subsequently, submonolayer Pt was controllably deposited on Pd_3Pb to obtain atomic-layer Pt/Pd_3Pb (AL-Pt/Pd_3Pb) (Figure 1D). It is reasonable that there were no new peaks assigned to Pt observed in the XRD pattern of AL-Pt/Pd_3Pb (Figure S1) compared with Pd_3Pb because the small proportion of Pt was below the detection limit of XRD. Despite the successful deposition of a submonolayer of Pt (Figure S5), the lattice spacing of 0.205 nm (Figure 1E) was still assigned to Pd_3Pb {200} facets because the substrate contributed the vast majority of the contrast degree. Since the brightness of an atom column in a HAADF-STEM image is dependent on the atomic number,[25,26] the brightness level of atoms should be Pb (82) > Pt (78) > Pd (46). As shown in Figures 1B and S6, the outermost surface of Pd_3Pb was terminated by Pd_1Pb_1 with a PdPbPdPb alignment, and a periodic light and dark contrast arrangement was observed. After the deposition of Pt, an obvious lighter layer covering the surface of Pd_3Pb was observed, and the periodic light and dark arrangement disappeared (Figure 1E). Hence, it is reasonable to conclude that the outermost layer of AL-Pt/Pd_3Pb was the atomic Pt layer. To further confirm the distribution, line intensity profiles along the yellow dashed arrow direction in Figure 1E were measured. As shown, the brightness of the outermost Pt atoms was clearly between those of Pb and Pd (Figure 1E_1,E_2). EDS mapping (Figure 1F) clearly displayed the Pd_3Pb core and the thin Pt shell, also confirming the outermost distribution of the Pt layer.

Since X-ray photoelectron spectroscopy (XPS) is an effective tool to reveal the electronic structure at the surface of catalysts,[27] XPS measurements were performed (Figure S7). Notably, the main peaks of Pb 4f in AL-Pt/Pd_3Pb shifted to higher binding energy compared with Pb in Pd_3Pb, along with a 0.2 eV left shift (Figure 2A). A similar peak shift to higher

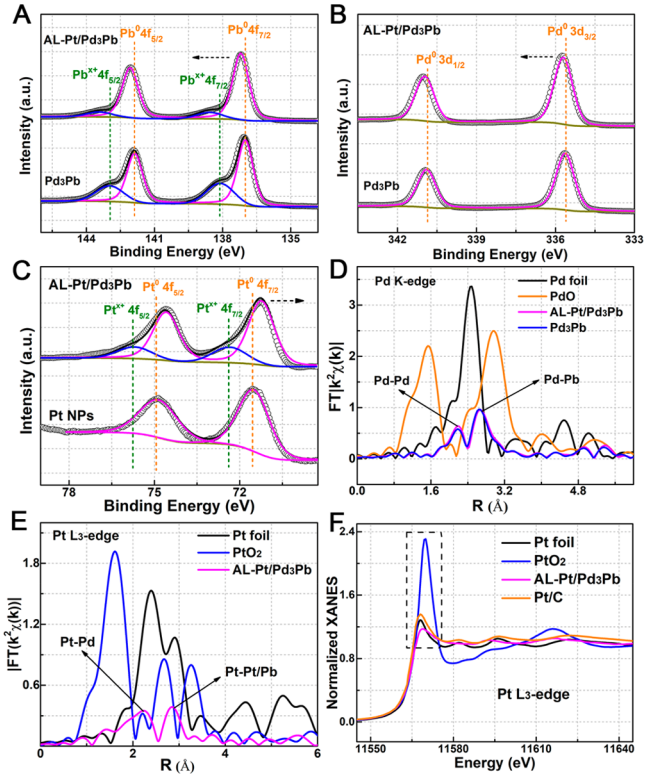

Figure 2. (A–C) XPS spectra of (A) Pb 4f, (B) Pd 3d, and (C) Pt 4f. (D, E) FT-EXAFS of (D) the Pd K-edge and (E) the Pt L_3-edge. (F) XANES of the Pt L_3-edge.

binding energy (0.15 eV left shift) was also observed for Pd 3d of AL-Pt/Pd_3Pb in comparison with Pd in Pd_3Pb (Figure 2B). As a contrast, the Pt 4f XPS spectrum of AL-Pt/Pd_3Pb (Figure 2C) shifted to lower binding energy (0.3 eV right shift) in comparison with Pt nanoparticles prepared using similar conditions as for Pd_3Pb (Figure S8). These results underlined the electron transfer from the Pd_3Pb substrate to the Pt layer.

Next, to further explore the local structure of AL-Pt/Pd_3Pb, the X-ray absorption fine structure (XAFS) was measured. The Fourier transform (FT) of the extended XAFS (EXAFS) of the Pd K-edge was almost coincident for AL-Pt/Pd_3Pb and Pd_3Pb (Figure 2D), indicating the similar coordination environments of Pd, and the strong peak at 2.65 Å was attributed to Pd–Pb coordination. The similarity of the Pb coordination environments in Pd_3Pb and AL-Pt/Pd_3Pb was also evidenced by the almost identical curves for the Pb L_2-edge (Figure S9). In the EXAFS spectrum of AL-Pt/Pd_3Pb, the Pt L_3-edge exhibited a peak at 2.17 Å belonging to the scattering of Pt–Pd and a peak at 2.64 Å corresponding to Pt–Pt/Pb coordination (Figure 2E). On the basis of the least-squares EXAFS fitting (Figures S10 and S11), the Pt coordination number was just 8.1 (Tables S1 and S2), which is far less than the saturated coordination

DOI: 10.1021/jacs.9b09391
J. Am. Chem. Soc. 2019, 141, 19964–19968

number of 12 in Pt foil. This result reinforced the existence of submonolayer Pt at the surface of Pd_3Pb. The X-ray absorption near-edge structure (XANES) shows that the white line intensity of Pt for AL-Pt/Pd_3Pb was below the intensity of Pt foil and commercial Pt/C (Figure 2F). This indicates that Pt exhibited partially negative valence, which resulted from the electron donation from the Pd_3Pb substrate to Pt. For Pb and Pd, the XANES analysis is shown in Figures S12 and S13.

Before electrocatalysis measurements, the catalysts underwent an annealing process at 400 °C for 12 h in an argon atmosphere to remove their covering surfactants (Figure S14).[28] To evaluate the HER activity of AL-Pt/Pd_3Pb, linear sweep voltammetry (LSV) was performed. As shown in Figures 3A and S15, AL-Pt/Pd_3Pb possessed a smaller onset potential

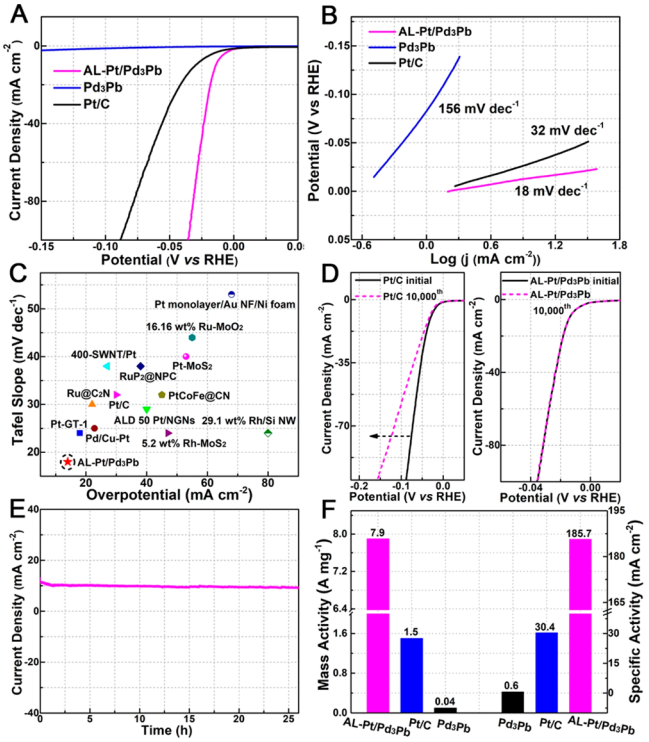

Figure 3. (A) Polarization curves. (B) Tafel slopes. (C) Comparison with different representative catalysts. (D) Durability test. (E) Chronoamperometry curve for AL-Pt/Pd_3Pb. (F) Specific activity and mass activity.

than Pt/C, Pd_3Pb, and Pt/Pd_3Pb alloy. In addition, we synthesized Pd_3Pb with different numbers of Pt layers and compared their acidic HER performance (Figure S16 and Table S3). Interestingly, AL-Pt/Pd_3Pb showed superior HER activity relative to Pd_3Pb with two Pt layers or three to four Pt layers. Besides the onset potential, only 13.8 mV (with *iR* correction based on Figure S17) was needed to reach 10 mA/cm^2 for AL-Pt/Pd_3Pb, which was much lower than for Pt/C (30 mV) and Pd_3Pb (296 mV). Next, we used the Tafel slope to evaluate the kinetics of samples during the HER (Figure 3B). Remarkably, the Tafel slope for AL-Pt/Pd_3Pb was just 18 mV/dec, which was much lower than that of Pt/C (30 mV/dec), suggesting faster kinetics of the reaction process. For comparison with reported precious metal HER catalysts in acidic media (using the overpotential at 10 mA/cm^2 and the Tafel slope for comparison), AL-Pt/Pd_3Pb presented almost the smallest overpotential and Tafel slope (Figure 3C and Table S4). Besides the activities, the stabilities of catalysts should also be taken into full consideration. After a 10 000 cycle electrochemical accelerated durability test (ADT), Pt/C exhibited 46% decay at 50 mA/cm^2, while AL-Pt/Pd_3Pb showed negligible activity decay (Figures 3D and S18). In addition, during a continuous 25 h chronoamperometry test at a potential of −14 mV, AL-Pt/Pd_3Pb also showed excellent stability (Figure 3E). At −0.05 V, the mass activity of AL-Pt/Pd_3Pb could reach to 7834 A/g (normalized to Pt and Pd), which was 5.3 times higher than that of Pt/C (1486 A/g) (Figure 3F). When normalized only to Pt, the mass activity of AL-Pt/Pd_3Pb actually reached 22 750 A/g, which is 15-fold higher than that of Pt/C. This was attributed to the maximized utilization of submonolayer Pt atoms on the surface of Pd_3Pb. The atomic-resolution HAADF-STEM image of the recycled sample (Figure S19) verified that the submonolayer Pt was still maintained after the durability test. In addition, the excellent stability of the Pd_3Pb substrate was also confirmed by the XRD spectra, EDS mapping, and HAADF-STEM image after the durability test (Figure S20).

DFT calculations were performed to explore the origin of the high HER activity of AL-Pt/Pd_3Pb. Figure 4A shows a clear

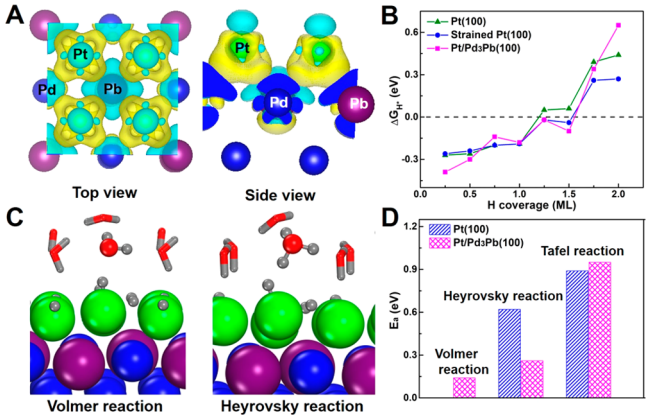

Figure 4. (A) Charge density difference (0.003 e/Å^3) of Pt and Pd_3Pb in Pt/Pd_3Pb(100). (B) Calculated differential free energy change of H*. (C) Optimized transition states for the Volmer and Heyrovsky reactions on Pt/Pd_3Pb. (D) Calculated barriers.

charge transfer from Pd and Pb to Pt, as evidenced by the electron accumulation (yellow areas) of Pt and the electron depletion (cyan areas) of Pd and Pb. The charge transfer caused an upshift of the Pt d-band center (~0.58 eV), resulting in stronger binding of H* on Pt/Pd_3Pb than on Pt(100) (Figure S21). We note that the electronic structure change of Pt can also be induced by the tensile strain of Pt (~3.6%) on Pd_3Pb due to the lattice misfit between Pt and Pd_3Pb. We found that the improved H* binding on Pt was mainly from the ligand effect of Pd_3Pb (Figure S21).

To understand how the electronic structure change of Pt affects the HER activity, the Gibbs free energy change of H* (ΔG_{H^*}) was calculated (Figure 4B). We found that ΔG_{H^*} was highly dependent on the coverage of H*, making the use solely of thermodynamics to evaluate the HER activity challenging. Thus, the kinetics of the elementary steps involved in the acidic HER was studied. Figure 4B suggests that the HER will start at a H* coverage of ~1.25−1.50 monolayer (ML) on both Pt(100) and Pt/Pd_3Pb. Thus, the surface covered by 1.50 ML of H* was used as an example to calculate the barriers. We

DOI: 10.1021/jacs.9b09391
J. Am. Chem. Soc. 2019, 141, 19964−19968

found that the Volmer reaction via proton transfer from H_3O^+ to the surface was a barrierless process on Pt(100) and was only required to pass a low barrier of 0.14 eV on Pt/Pd_3Pb (Figures 4C and S22). At the transition state of the Heyrovsky reaction, H*/Pt was pulled out ~0.05 Å on Pt/Pd_3Pb, which is much smaller than the value of ~0.60 Å on Pt(100), since H*/Pt on Pt/Pd_3Pb was stabilized by the electrostatic interaction between the negatively charged Pt and positively charged Pd and Pb. This resulted in a lower barrier of 0.26 eV on Pt/Pd_3Pb compared with 0.62 eV on Pt(100). The barriers for the Heyrovsky reaction were much lower than that for Tafel reaction on these two surfaces (Figure 4D), suggesting that the HER was prone to proceed via the Volmer–Heyrovsky mechanism, consistent with the reported experimental results.[29] On the other hand, it was reported that the acidic HER on a Pt catalyst was less structure-sensitive,[30,31] and therefore, the lower barrier of the rate-limiting Heyrovsky reaction on Pt/Pd_3Pb compared with Pt(100) indicated that Pt/Pd_3Pb exhibited a higher HER activity than Pt, in line with our experiments (Figure 3A).

In summary, submonolayer Pt was successfully deposited on intermetallic Pd_3Pb nanoplates. The intermetallic substrate can stabilize the atomic structure of the active Pt layer and guarantee its long-term operation in the acidic HER process. The modulation of the electronic structure by the electron transfer from Pd_3Pb to Pt also results in superior HER activity of AL-Pt/Pd_3Pb. Our findings highlight the ability of surface engineering at the atomic scale to enable extreme utilization of precious metals for energy conversion.

■ ASSOCIATED CONTENT

Supporting Information

The Supporting Information is available free of charge at https://pubs.acs.org/doi/10.1021/jacs.9b09391.

Detailed experimental procedures, TEM images, electron diffraction pattern, AFM image, XRD patterns, EDS spectra, XPS spectra, XANES spectra, EIS curves, specific activity data, and EXAFS fitting results (PDF)

■ AUTHOR INFORMATION

Corresponding Author

*yuenwu@ustc.edu.cn

ORCID

Xiang-Kui Gu: 0000-0001-6537-7026
Tao Yao: 0000-0001-8699-8294
Yue Lin: 0000-0001-5333-511X
Hai Li: 0000-0002-9659-1153
Xun Hong: 0000-0003-2784-2868
Shiqiang Wei: 0000-0002-2052-1132
Wei-Xue Li: 0000-0002-5043-3088
Yadong Li: 0000-0003-1544-1127
Yuen Wu: 0000-0001-9524-2843

Author Contributions

○Y.Y., X.-K.G., and D.H. contributed equally.

Notes

The authors declare no competing financial interest.

■ ACKNOWLEDGMENTS

We thank the photoemission endstations BL1W1B at the Beijing Synchrotron Radiation Facility (BSRF), BL14W1 at the Shanghai Synchrotron Radiation Facility (SSRF), and BL10B and BL11U at the National Synchrotron Radiation Laboratory (NSRL) for the help in characterizations. This work was supported by the National Key R&D Program of China 2017YFA (0208300 and 0700100) and the National Natural Science Foundation of China (21522107, 21671180, 21521091, and U1463202).

■ REFERENCES

(1) Palo, D. R.; Dagle, R. A.; Holladay, J. D. Methanol steam reforming for hydrogen production. *Chem. Rev.* **2007**, *107*, 3992.
(2) Navarro, R. M.; Pena, M. A.; Fierro, J. L. G. Hydrogen production reactions from carbon feedstocks: fossil fuels and biomass. *Chem. Rev.* **2007**, *107*, 3952.
(3) Gu, X.-K.; Li, W. X. First-principles study on the origin of the different selectivities for methanol steam reforming on Cu (111) and Pd (111). *J. Phys. Chem. C* **2010**, *114*, 21539.
(4) Gu, X.-K.; Qiao, B.; Huang, C.-Q.; Ding, W.-C.; Sun, K.; Zhan, E.; Zhang, T.; Liu, J.; Li, W.-X. Supported Single Pt_1/Au_1 Atoms for Methanol Steam Reforming. *ACS Catal.* **2014**, *4*, 3886.
(5) Greeley, J.; Jaramillo, T. F.; Bonde, J.; Chorkendorff, I. B.; Nørskov, J. K. Computational high-throughput screening of electrocatalytic materials for hydrogen evolution. *Nat. Mater.* **2006**, *5*, 909.
(6) Zheng, Y.; Jiao, Y.; Jaroniec, M.; Qiao, S. Z. Advancing the electrochemistry of the hydrogen-evolution reaction through combining experiment and theory. *Angew. Chem., Int. Ed.* **2015**, *54*, 52.
(7) Yao, Y.; Hu, S.; Chen, W.; Huang, Z.-Q.; Wei, W.; Yao, T.; Liu, R.; Zang, K.; Wang, X.; Wu, G.; et al. Engineering the electronic structure of single atom Ru sites via compressive strain boosts acidic water oxidation electrocatalysis. *Nat. Catal.* **2019**, *2*, 304.
(8) Zheng, Y.; Jiao, Y.; Vasileff, A.; Qiao, S. Z. The hydrogen evolution reaction in alkaline solution: from theory, single crystal models, to practical electrocatalysts. *Angew. Chem., Int. Ed.* **2018**, *57*, 7568.
(9) Li, M.; Ma, Q.; Zi, W.; Liu, X.; Zhu, X.; Liu, S. F. Pt monolayer coating on complex network substrate with high catalytic activity for the hydrogen evolution reaction. *Sci. Adv.* **2015**, *1*, No. e1400268.
(10) Morales-Guio, C. G.; Stern, L. A.; Hu, X. Nanostructured hydrotreating catalysts for electrochemical hydrogen evolution. *Chem. Soc. Rev.* **2014**, *43*, 6555.
(11) Subbaraman, R.; Tripkovic, D.; Strmcnik, D.; Chang, K.-C.; Uchimura, M.; Paulikas, A. P.; Stamenkovic, V.; Markovic, N. M. Enhancing hydrogen evolution activity in water splitting by tailoring Li^+-Ni(OH) $_2$-Pt interfaces. *Science* **2011**, *334*, 1256.
(12) Cheng, N.; Stambula, S.; Wang, D.; Banis, M. N.; Liu, J.; Riese, A.; Xiao, B.; Li, R.; Sham, T.-K.; Liu, L.-M.; Botton, G. A.; Sun, X. Platinum single-atom and cluster catalysis of the hydrogen evolution reaction. *Nat. Commun.* **2016**, *7*, 13638.
(13) Yu, W.; Porosoff, M. D.; Chen, J. G. Review of Pt-based bimetallic catalysis: from model surfaces to supported catalysts. *Chem. Rev.* **2012**, *112*, 5780.
(14) Stamenkovic, V. R.; Fowler, B.; Mun, B. S.; Wang, G.; Ross, P. N.; Lucas, C. A.; Marković, N. M. Improved oxygen reduction activity on Pt_3Ni (111) via increased surface site availability. *Science* **2007**, *315*, 493.
(15) Chao, T.; Luo, X.; Chen, W.; Jiang, B.; Ge, J.; Lin, Y.; Wu, G.; Wang, X.; Hu, Y.; Zhuang, Z.; Wu, Y.; Hong, X.; Li, Y. Atomically dispersed copper–platinum dual sites alloyed with palladium nanorings catalyze the hydrogen evolution reaction. *Angew. Chem., Int. Ed.* **2017**, *56*, 16047.
(16) Zhang, J.; Zhao, Y.; Guo, X.; Chen, C.; Dong, C.-L.; Liu, R.-S.; Han, C.-P.; Li, Y.; Gogotsi, Y.; Wang, G. Single platinum atoms immobilized on an MXene as an efficient catalyst for the hydrogen evolution reaction. *Nat. Catal.* **2018**, *1*, 985.
(17) Liu, Y.; Gokcen, D.; Bertocci, U.; Moffat, T. P. Self-terminating growth of platinum films by electrochemical deposition. *Science* **2012**, *338*, 1327.
(18) Wang, X.; Choi, S.-I.; Roling, L. T.; Luo, M.; Ma, C.; Zhang, L.; Chi, M.; Liu, J.; Xie, Z.; Herron, J. A.; Mavrikakis, M.; Xia, Y.

DOI: 10.1021/jacs.9b09391
J. Am. Chem. Soc. 2019, 141, 19964–19968

Palladium−platinum core-shell icosahedra with substantially enhanced activity and durability towards oxygen reduction. *Nat. Commun.* **2015**, *6*, 7594.
(19) Meier, J. C.; Galeano, C.; Katsounaros, I.; Topalov, A. A.; Kostka, A.; Schüth, F.; Mayrhofer, K. J. Degradation mechanisms of Pt/C fuel cell catalysts under simulated start−stop conditions. *ACS Catal.* **2012**, *2*, 832.
(20) Yang, X. F.; Wang, A.; Qiao, B.; Li, J.; Liu, J.; Zhang, T. Single-atom catalysts: a new frontier in heterogeneous catalysis. *Acc. Chem. Res.* **2013**, *46*, 1740.
(21) Pallassana, V.; Neurock, M.; Hansen, L. B.; Hammer, B.; Nørskov, J. K. Theoretical analysis of hydrogen chemisorption on Pd(111), Re(0001) and Pd_{ML}/Re(0001), Re_{ML}/Pd(111) pseudomorphic overlayers. *Phys. Rev. B: Condens. Matter Mater. Phys.* **1999**, *60*, 6146.
(22) Seh, Z. W.; Kibsgaard, J.; Dickens, C. F.; Chorkendorff, I. B.; Nørskov, J. K.; Jaramillo, T. F. Combining theory and experiment in electrocatalysis: Insights into materials design. *Science* **2017**, *355*, eaad4998.
(23) Casado-Rivera, E.; Volpe, D. J.; Alden, L.; Lind, C.; Downie, C.; Vázquez-Alvarez, T.; Angelo, A. C.; DiSalvo, F. J.; Abruna, H. D. Electrocatalytic activity of ordered intermetallic phases for fuel cell applications. *J. Am. Chem. Soc.* **2004**, *126*, 4043.
(24) Yan, Y.; Du, J. S.; Gilroy, K. D.; Yang, D.; Xia, Y.; Zhang, H. Intermetallic nanocrystals: Syntheses and catalytic applications. *Adv. Mater.* **2017**, *29*, 1605997.
(25) Li, J.; Yin, H.-M.; Li, X.-B.; Okunishi, E.; Shen, Y.-L.; He, J.; Tang, Z.-K.; Wang, W.-X.; Yücelen, E.; Li, C.; et al. Surface evolution of a Pt−Pd−Au electrocatalyst for stable oxygen reduction. *Nat. Energy* **2017**, *2*, 17111.
(26) Kothleitner, G.; Neish, M. J.; Lugg, N. R.; Findlay, S.; Grogger, W.; Hofer, F.; Allen, L. J. Quantitative elemental mapping at atomic resolution using X-ray spectroscopy. *Phys. Rev. Lett.* **2014**, *112*, 085501.
(27) Choudhury, D.; Das, B.; Sarma, D. D.; Rao, C. N. R. XPS evidence for molecular charge-transfer doping of graphene. *Chem. Phys. Lett.* **2010**, *497*, 66.
(28) Chen, C.; Kang, Y.; Huo, Z.; Zhu, Z.; Huang, W.; Xin, H. L.; Snyder, J. D.; Li, D.; Herron, J. A.; Mavrikakis, M.; Chi, M.; More, K. L.; Li, Y.; Markovic, N. M.; Somorjai, G. A.; Yang, P.; Stamenkovic, V. R. Highly crystalline multimetallic nanoframes with three-dimensional electrocatalytic surfaces. *Science* **2014**, *343*, 1339.
(29) Marković, N. M.; Grgur, B. N.; Ross, P. N. Temperature-dependent hydrogen electrochemistry on platinum low-index single-crystal surfaces in acid solutions. *J. Phys. Chem. B* **1997**, *101*, 5405.
(30) Kita, H.; Ye, S.; Gao, Y. Mass transfer effect in hydrogen evolution reaction on Pt single-crystal electrodes in acid solution. *J. Electroanal. Chem.* **1992**, *334*, 351.
(31) Gomez, R.; Fernandez-Vega, A.; Feliu, J. M.; Aldaz, A. J. Hydrogen Evolution on Pt Single Crystal Surfaces: Effects of Irreversibly Adsorbed Bismuth and antimony on Hydrogen Adsorption and Evolution on Pt(100). *J. Phys. Chem.* **1993**, *97*, 4769.

DOI: 10.1021/jacs.9b09391
J. Am. Chem. Soc. 2019, 141, 19964−19968